Hygroscopic Growth and Deliquescence of NaCl Nanoparticles Mixed with Surfactant SDS

Christopher W. Harmon,[†] Ronald L. Grimm,[†] Theresa M. McIntire,[†] Mark D. Peterson,[†] Bosiljka Njegic,[†] Vanessa M. Angel,[†] Ahmad Alshawa,[†] Joelle S. Underwood,[†,‡] Douglas J. Tobias,[†] R. Benny Gerber,[†,§] Mark S. Gordon,[∥] John C. Hemminger,[†] and Sergey A. Nizkorodov*[,†]

Department of Chemistry, University of California, Irvine, California 92697-2025; Institute of Chemistry, The Hebrew University of Jerusalem, Jerusalem 91904, Israel; and Department of Chemistry, Iowa State University, Ames, Iowa 50011-3111

Received: October 8, 2009; Revised Manuscript Received: January 5, 2010

Several complementary experimental and theoretical methodologies were used to explore water uptake on sodium chloride (NaCl) particles containing varying amounts of sodium dodecyl sulfate (SDS) to elucidate the interaction of water with well-defined, environmentally relevant surfaces. Experiments probed the hygroscopic growth of mixed SDS/NaCl nanoparticles that were generated by electrospraying aqueous 2 g/L solutions containing SDS and NaCl with relative NaCl/SDS weight fractions of 0, 5, 11, 23, or 50 wt/wt %. Particles with mobility-equivalent diameters of 14.0(±0.2) nm were size selected and their hygroscopic growth was monitored by a tandem nano-differential mobility analyzer as a function of relative humidity (RH). Nanoparticles generated from 0 and 5 wt/wt % solutions deliquesced abruptly at 79.1(±1.0)% RH. Both of these nanoparticle compositions had 3.1(±0.5) monolayers of adsorbed surface water prior to deliquescing and showed good agreement with the Brunauer−Emmett−Teller and the Frenkel−Halsey−Hill isotherms. Above the deliquescence point, the growth curves could be qualitatively described by Köhler theory after appropriately accounting for the effect of the particle shape on mobility. The SDS/NaCl nanoparticles with larger SDS fractions displayed gradual deliquescence at a RH that was significantly lower than 79.1%. All compositions of SDS/NaCl nanoparticles had monotonically suppressed mobility growth factors (GF_m) with increasing fractions of SDS in the electrosprayed solutions. The Zdanovskii−Stokes−Robinson model was used to estimate the actual fractions of SDS and NaCl in the nanoparticles; it suggested the nanoparticles were enhanced in SDS relative to their electrospray solution concentrations. X-ray photoelectron spectroscopy (XPS), FTIR, and AFM were consistent with SDS forming first a monolayer and then a crystalline phase around the NaCl core. Molecular dynamics simulations of water vapor interacting with SDS/NaCl slabs showed that SDS kinetically hinders the initial water uptake. Large binding energies of sodium methyl sulfate (SMS)−$(NaCl)_4$, H_2O−$(NaCl)_4$, and SMS−H_2O−$(NaCl)_4$ calculated at the MP2/cc-pVDZ level suggested that placing H_2O in between NaCl and surfactant headgroup is energetically favorable. These results provide a comprehensive description of SDS/NaCl nanoparticles and their properties.

Introduction

Thin water films are ubiquitous on many common environmental surfaces including atmospheric particles.[1] In many instances, these thin films are responsible for macroscopic observations, even though they may only constitute a very small fraction of the system's total mass or volume. Thin water films on atmospheric particles participate in a variety of chemical reactions and physical interactions including the nucleation of cloud droplets.[2] Thus, it is critical to understand the fundamental interactions of water with atmospheric aerosol including the relative humidity at which solid particles deliquesce, as well as the effects of particle size and chemical composition on hygroscopic properties.

NaCl has routinely been used as a model system for sea-salt aerosols.[3] Previous measurements on bulk crystalline NaCl showed that above 70% relative humidity (RH), 3.5−4.0 monolayers (ML) of water are adsorbed onto the surface.[1,3,4] As the RH above the NaCl surface increases, enough water adsorbs to the surface to initiate a deliquescence transition from the crystalline to aqueous phase at the deliquescence relative humidity (DRH).[1] Measurements in several laboratories including this one[5−12] showed that DRH values for NaCl particles less than 100 nm in size are higher than the DRH of 75% measured for larger NaCl particles (>100 nm) and bulk NaCl.[13] This size dependence originates from the surface tension contribution of the thin water film to the system's free energy, which for small enough particles is comparable in magnitude to that from the NaCl bulk. This changes the Gibbs free energy of deliquescence such that more water vapor above the surface is required to initiate the deliquescence.[12] Consequently, as the size of the dry nanoparticle decreases, its DRH increases.[10,12]

Numerous studies have addressed the effects of organic material on the hygroscopic properties of inorganic particles.[5,14−21] Researchers often assume that organic/inorganic particles will phase segregate into a "core-shell" morphology with an organic "shell" coating an inorganic crystalline "core" as shown in the

* Corresponding author. E-mail: nizkorod@uci.edu.
[†] University of California.
[‡] Current address: Department of Chemistry, Loyola University, New Orleans, LA 70118.
[§] The Hebrew University of Jerusalem.
[∥] Iowa State University.

10.1021/jp909661q
Published on Web 01/28/2010

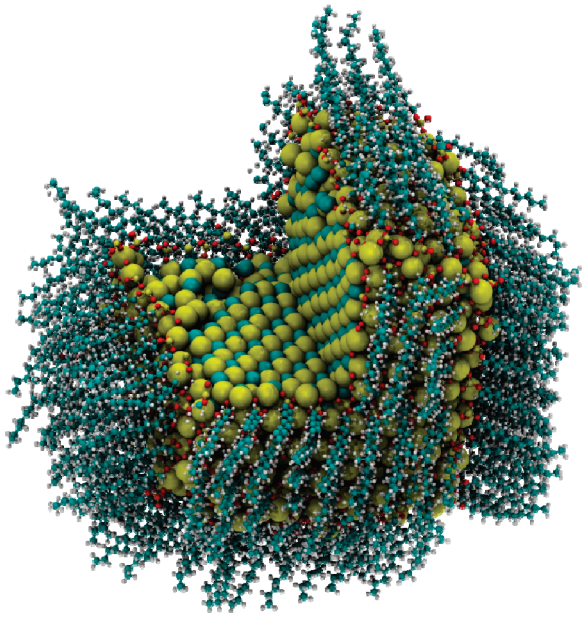

Figure 1. A NaCl core−SDS shell nanoparticle relaxed by a 100 ps MD simulation. For the display purposes, a section of the particle is cut away to reveal the inner structure of the NaCl core. Significant distortions of the NaCl crystalline structure are observed on the corners and edges of the NaCl cube.

illustration in Figure 1. Observations show that the organic coating does not always inhibit growth of the soluble inorganic core, even for cases in which the organic material comprised the majority of the particle mass.[14,15] In many cases, water uptake can be accurately predicted by the Zdanovskii−Stokes−Robinson (ZSR) model, which assumes the individual particle constituents adsorb water independently in proportion to their volume fraction.[16,17] As poorly soluble organics are not expected to take up any measurable amount of water at humidities between 5 and 95%, the soluble inorganic core is therefore expected to contribute solely to hygroscopic growth of mixed particles.[5] The situation is somewhat more complicated for particles containing sparingly soluble organics, where the presence of organics can affect both the degree of the water uptake and DRH for the inorganic core. For example, Chen and Lee noted a shift in the deliquescence point to lower RH for 100 nm NaCl particles mixed with glutaric and pyruvic acid.[20] Woods et al. found that deliquescence was shifted to lower humidity by ∼1% RH for 100 nm NaCl particles with roughly one coverage layer of sodium dodecyl sulfate (SDS).[18] In this laboratory, experiments on mixed sodium bis(2-ethylhexyl) sulfosuccinate (AOT)/NaCl nanoparticles (9 and 14 nm in mobility equivalent diameter) measured the onset of deliquescence at significantly lower RH (up to 10% lower) than for pure NaCl particles of the same size. Results were attributed to interactions between $NaCl-H_2O-Na^+$ and $^-O_3SO-R$ at the surface that were comparable to the magnitude of the Na−Cl binding energy.[5] These results suggest the surfactants affect the deliquescence of NaCl in a size-dependent way and motivate the present investigation of hygroscopicity of mixed SDS/NaCl nanoparticles.

Typical minimum cloud condensation nuclei (CCN) activation diameters at 100.5% RH are 20−30 nm for soluble inorganics, such as NaCl, and 100−200 nm for weakly soluble organics, such as SDS.[22] Furthermore, field measurements show marine-based aerosols are typically in the micrometer size regime.[23] The size of particles studied in this work is therefore not representative of the real atmosphere. However, we elect to study nanoparticles because of their unique surface properties. There is also an experimental advantage to studying nanoparticles: the surfactant and water coating on predeliquesced aerosol is a larger and more easily quantifiable fraction of the total diameter than for larger particles.

Herein, we present a combined experimental and computational investigation designed to gain a comprehensive picture of the hygroscopic growth of hybrid surfactant−NaCl nanoparticles. SDS is chosen as a model single-chain surfactant. Computational investigations include molecular dynamics (MD) simulations to visualize how adsorbed water interacts with SDS/NaCl slabs as well as high-level *ab initio* calculations to characterize the structural and energetic aspects of interactions between NaCl, H_2O, and SDS. Experimental investigations include tandem nano-differential mobility analysis (DMA) to characterize the water uptake by the size-selected SDS/NaCl nanoparticles generated by electrospraying a solution containing SDS and NaCl. Activity measurements (see discussion below) over bulk mixtures of NaCl and SDS are conducted to compare to nanoparticle hygroscopic growth. X-ray photoelectron spectroscopy (XPS), FTIR, and atomic force microscopy (AFM) are used to characterize the dry nanoparticle composition and morphology. Table 1 serves as a guide for the techniques employed in this work, their application, and the range of the SDS content these techniques probe.

Experimentally, water uptake and deliquescence can be characterized using the mobility growth factor GF_m, defined in eq 1 as a ratio of the wet mobility diameter $d_m(RH)$ to that of the dry mobility diameter $d_m(0)$. Mobility diameters are typically quantified using tandem DMA techniques.[24,25]

$$GF_m = \frac{d_m(RH)}{d_m(0)} \quad (1)$$

This macroscopic metric of water uptake may not seem appropriate for nanoparticles given that their size can be on the order of molecular dimensions. However, GF_m and DRH can still be accurately predicted for single component soluble inorganic nanoparticles using bulk thermodynamic treatments

TABLE 1: Techniques Employed in this Work and their Applications

technique	provides information about	wt/wt % SDS/NaCl or SDS coverage probed
tandem hygroscopic growth	equilibrium water uptake by nanoparticles	0−90%
water vapor activity	equilibrium water uptake by bulk mixtures	0−100%
MD simulations	qualitative visualization of dynamics of the initial water uptake by the NaCl/SDS surfaces	<1.0 monolayer
ab initio calculations	binding energies and interactions between NaCl clusters, H_2O, and SDS	individual molecules and small clusters
AFM imaging	morphology and size of NaCl/SDS nanoparticles	23%
FTIR spectroscopy	phase state of SDS in the nanoparticles	23%
XPS spectroscopy	relative amounts of SDS/NaCl in the nanoparticles	0−50%

TABLE 2: Electrospray Conditions and Particle Size Characteristics for Various SDS/NaCl Solutions Used in This Work

wt/wt % SDS/NaCl[a]	χ_{NaCl}[b]	total solution concn (g L^{-1})	applied potential (kV)	flow rate (μL h^{-1})	l_s (mm)[c]	d_m (nm)[d]	particle concn ($\times 10^5$ cm^{-3})	GSD[e]
0.0	1.00	1.52	3.4	109	4.0	15.2	0.67	1.29
5.0	0.99	1.98	3.2	83	4.0	15.2	0.57	1.27
11	0.98	2.05	3.1	81	5.0	15.5	0.67	1.26
23	0.94	1.93	3.2	81	4.0	17.9	1.04	1.36
50	0.83	2.03	3.1	81	6.0	24.5	1.43	1.33

[a] Dry weight percent of SDS in solution containing 2 g/L total of SDS and NaCl. [b] Dry mol fraction of NaCl in solution. [c] Electrospray distance from capillary tip to neutralizer entrance. [d] Geometric mean mobility diameter of electrosprayed nanoparticles prior to the size selection. [e] Geometric standard deviation (GSD) prior to the size selection.

when properly accounting for particle shape.[9,11,12] Köhler theory has previously been used to predict GF_m for NaCl nanoparticles[9] and will be used to interpret GF_m data for NaCl and SDS/NaCl nanoparticles in this work.

Upon deliquescence, NaCl particles become saturated aqueous solutions and subsequently dilute as they take up more water. Due to the nonideality associated with concentrated electrolyte solutions, vapor pressure, solubility, free energy of mixing, freezing-point depression, boiling-point elevation, and osmotic pressure must be determined experimentally.[26] Water activity a_w is often used in association with equilibrium vapor pressure $p_{vap,aq}$ over nonideal aqueous solutions. Equation 2 shows water activity for bulk liquids and eq 3 for particles with small diameters, which includes a Kelvin effect correction term $C_K(\sigma_{aq},d_m)$.

$$a_w = \frac{p_{vap,aq}}{p^0_{vap,H_2O}} = \frac{RH}{100} \quad (2)$$

$$a_w C_K(\sigma_{aq}, d_m) = \frac{RH}{100} = a_w \exp\left(\frac{4M_w\sigma_{aq}(w_t)}{RT\rho_{aq}(w_t)d_m(RH)}\right) \quad (3)$$

M_w is the molecular weight of water and $d_m(RH)$ is the particle diameter (which changes with RH in our experiments). Activity $a_w(w_t)$, density $\rho_{aq}(w_t)$, and surface tension $\sigma_{aq}(w_t)$ of the electrolyte solution have been determined experimentally as a function of $NaCl_{(aq)}$ weight percent w_t for $0 < w_t < 45\%$.[27,28] Surface tensions over NaCl and NaCl solution have been shown to decrease with size, and corrections to account for this are available in the literature.[29,30] However, these corrections are significant only for particles below ~10 nm in size. Therefore, they were not included in eq 3 in order to simplify the calculations for the 14 nm particles studied in this work.

As NaCl particles are not spherical, appropriate shape corrections are required in order to relate their mobility equivalent diameter and their actual size. Equation 4 corresponds to "Model 4" from Biskos et al.,[9] which is a version of Köhler theory from Cinkotai et al.[31] with an inclusion of shape effects on particle mobility.

$$GF_m = \left(\frac{100\rho_s}{w_t(a_w)\rho_{aq}(w_t)}\right)^{1/3} A(Kn,\chi_v) \quad (4)$$

ρ_s is the density of $NaCl_{(S)}$ (2163 kg m^{-3}) and $A(Kn,\chi_v)$ is a shape effect correction function of Knudsen number Kn and free-molecular regime shape factor χ_v, which has been calculated iteratively in a previous publication.[5] The term $A(Kn,\chi_v)$ has a unique solution in each flow regime which satisfies the relationship in eq 5, where $d_e(0)$ is the envelop equivalent, often referred to as volume equivalent diameter under dry conditions.

$$d_e(0) = A(Kn,\chi_v)d_m(0) \quad (5)$$

It was found that the experimentally measured GF_m could be predicted reasonably well by use of Köhler theory for NaCl particles between 6 and 60 nm, provided the correct flow regime was used for a particle of a given Knudsen number.[9] The critical parameter in the Köhler theory analysis is the surface tension−diameter relationship provided by the Kelvin effect. By purposely adding molecules that affect this surface tension (i.e., surfactants), DRH and hygroscopic growth are expected to be altered significantly. The goal of this research is to understand at a fundamental level the effect of surfactants on hygroscopic growth of NaCl nanoparticles both below and above the deliquescence transition in NaCl.

Experimental Methods

Generation of NaCl and SDS/NaCl Nanoparticles. NaCl and SDS/NaCl nanoparticles were generated with an electrospray particle generator, designed in-house and described in detail elsewhere.[5,32] Variable amounts of NaCl (Sigma-Aldrich, 99.999%) and SDS (Fluka, ≥99.0%) were dissolved in HPLC grade water (OmniSolv, <8 $\mu\Omega\cdot$cm) and a small amount (<5%) of methanol (HPLC grade, Sigma-Aldrich) to achieve a combined NaCl + SDS weight concentration of ~2 g L^{-1}. Solutions were pushed through a 100 μm capillary from a syringe pump operating at a typical flow rate of ~1 μL min^{-1} with a ~3 kV positive potential applied to the stainless steel tip of the syringe. The electrospray was operated in a stable cone-jet mode and generated a dry polydisperse population of particles with number density of the order of 10^5 cm^{-3}. The size characteristics of the initial particle distribution from the electrospray source were sensitive functions of applied voltage, syringe pump flow rate, and distance (l_s) from the capillary tip to the electrically grounded neutralizer entrance. Table 2 summarizes the electrospray conditions and typical particle size characteristics that resulted from the varying solution compositions. These conditions represent optimized electrospray protocols for sustaining the cone-jet mode over long periods of time (~6 h). The final relative SDS/NaCl concentration in the nanoparticles is a function of the electrospray dynamics and is unknown a priori. Consequently, the various compositions of SDS/NaCl nanoparticles will be referred to by the solution composition from which they were generated and all values refer to the relative weight percents of SDS relative to NaCl (wt/wt %).

Hygroscopic Growth Measurements of NaCl and SDS/NaCl Nanoparticles. Nanoparticles were size selected and their hygroscopic growth was monitored by use of tandem-nano differential mobility analysis techniques, described previously.[5,10] A fixed voltage was applied to the first differential mobility analyzer (DMA1) under dry conditions (RH < 1.0% at 295 K) located downstream from the neutralizer, which selected a narrow distribution (geometric standard deviation, GSD ~1.05) from the initial populations shown in Table 2. The electrospray was operated continuously, RH was increased gradually, and the d_m(RH) distribution was monitored throughout the course of experimentation by a humidified, scanning DMA (DMA2) connected to an optical particle counter.

A custom LabView program was used to monitor the signal from Vaisala HMP237 RH probes. GF_m are reported in this paper as a function of the final RH encountered by particles in the DMA2 sheath flow. All RH probes were calibrated against the vapor pressure over saturated salt solutions. In some experiments DMA2 was maintained roughly 3% RH above the environment between DMAs 1 and 2. Particles therefore were only exposed to the final RH value for the time they spend inside the DMA2 column (~1 s). In other experiments particles were exposed to 7 and 67 s of RH. This was achieved by using a uniform RH throughout the entire particle flow, including DMA2, and increasing the length and volume of the humidified environment between DMAs 1 and 2.

Bulk Measurements of H_2O Activity over NaCl/Na_2SO_4 and NaCl/SDS. Equilibrium vapor pressures over bulk saturated solutions containing NaCl and SDS were also measured. Similar measurements were conducted for the mixture of NaCl and Na_2SO_4 for validation purposes. Solutions were prepared in a 280 cm^3 Vaisala HMK15 humidity calibrator chamber and allowed to equilibrate for 24 h before measurement with Vaisala HMP237 humidity probes. RH probes were calibrated as previously described for nanoparticles experiments. In these studies, 3.00 g of total material (NaCl and SDS or NaCl and Na_2SO_4) mixed in varying proportions and ground to a fine powder was immersed in 5.00 mL of HPLC grade water (OmniSolv, <8 $\mu\Omega\cdot$cm) followed by sonication. After an initial equilibration for 24 h, RH probes were inserted in the O-ring sealed chamber ports and humidities were reported after 1 h probe exposure when the humidity was less than 90% RH and after 12 h when the humidity was greater than 90% RH.

Characterization of Dry SDS/NaCl Nanoparticles. In a separate set of experiments, dry nanoparticles prepared from each SDS/NaCl solution were collected from the electrospray source using a home-built nanoparticle jet impactor based on the design of De La Mora et al.[33,34] The nanoparticle beam was expanded into an evacuated region at ~25 Torr through a 200 μm pinhole where a suitable substrate for impaction was located ~5 mm downstream. The flow through the pinhole was 330 sccm (standard cubic centimeters per minute); all the excess flow from the electrospray particle generator was vented. This impactor collected nanoparticles for physical imaging using AFM and chemical analysis using X-ray photoelectron spectroscopy (XPS) and FTIR.

XPS (VG Scientific Ltd.) analysis was carried out on the full particle distribution (Table 2) emerging directly from the electrospray particle source for each composition to maximize the measured XPS signal. Nanoparticles were impacted on highly ordered pyrolytic graphite (HOPG, Union Carbide) for roughly 6 h, after which time a deposition ring approximately 0.5 mm in diameter was visible on the substrate surface. The XPS experiments were carried out under ultrahigh vacuum conditions with base pressures below 1 nanoTorr. Incident photons were generated from an Al Kα source operating at 14 kV and 34 mA. The HOPG substrate was positioned such that the nanoparticle ring was centered directly under the optimized position for sampling by the electron energy analyzer, which was set to 20 eV for all experiments. Sulfur S(2p) and chlorine Cl(2p) photoelectrons were analyzed as proxies for SDS and NaCl, respectively, with identical step sizes and dwell times for comparison.

Samples of SDS/NaCl nanoparticle material were impacted on ZnSe windows (Edmund Optics) and were monitored using transmission FTIR spectroscopy. Infrared spectra were collected over the spectral range of interest, 4000−650 cm^{-1}, as single-beam spectra at 4 cm^{-1} resolution using 2560 scans for both the background and sample spectra, respectively, with a Nicolet AVATAR FTIR instrument (now Thermo Electron Corp., Madison, WI). Infrared absorption spectra were obtained by ratioing the single-beam spectra of the deposited nanoparticle material to the background spectrum of a clean zinc selenide window (CVD ZnSe, Cradley Crystals Corp.). Particle impaction time for FTIR analysis was also 6 h, after which time a visible particle deposition ring was present on the ZnSe window. Prior to analysis, impacted nanoparticle material remained in the FTIR chamber for several days under dry conditions (<1% RH at 295 K) until gas-phase water bands were no longer visible and degassing of water from the collected particles had thus ceased. FTIR spectra were only collected for the dried SDS/NaCl nanoparticles; interference from gas-phase water prevented us from getting reliable spectra of wet particles.

Samples of SDS/NaCl nanoparticle material impacted on HOPG or mica were imaged at ambient pressure and humidity using a Park Scientific Instruments AutoProbe CP Research (now Veeco Metrology Inc., Santa Barbara, CA) scanning probe microscope in intermittent contact mode. As AFM analysis required significantly fewer particles, collection times of 30−45 min were typically employed and particles were size selected by DMA prior to the impaction. AFM images were acquired using highly doped silicon tips (BudgetSensors) with a force constant of 3 N/m in intermittent contact mode. The 5 μm piezoelectric scanner was calibrated in the xy directions using a grating and in the z direction using several conventional height standards. Topographs were obtained as 256 × 256 pixels, flattened line-by-line and analyzed using the AutoProbe image processing software. AFM images of nanoparticles were taken under ambient conditions at 295 K and ~40% RH. It is therefore expected that all imaged nanoparticles have a thin surface layer of water, which may contribute to the imaged morphology.

Molecular Dynamics. SDS/NaCl slabs were generated consisting of either a crystalline NaCl core or an aqueous NaCl solution core that were decorated by SDS molecules. Individual slabs were generated in an $x-y-z$ periodic simulation box of dimensions $x = 39.40$ Å, $y = 39.40$ Å, $z = 200.00$ Å. Varying the number of SDS molecules in individual slabs simulated the effect of a varying coverage layer (Θ_{SDS}) of SDS on NaCl nanoparticles in the limit of 0.0 ML < $\Theta_{SDS} \leq$ 1.0 ML.

The NaCl crystalline core was generated manually using a standard NaCl crystal structure with a lattice constant of 5.63 Å, which gave a nearest-neighbor spacing of 2.81 Å. A full coverage monolayer of dodecyl sulfate anions (DS^-) was arranged in a rectangular lattice 5.00 Å apart on the NaCl slab with an appropriate number of sodium cation counterions. This defined the slab with $\Theta_{SDS} = 1.00$ ML while five additional slabs were generated by increasing the monolayer spacing constant to achieve $\Theta_{SDS} = 0.00$, 0.25, 0.40, 0.60, and 0.80

ML. SDS molecules were positioned such that the sulfur was placed 6.61 Å above the surface of the NaCl slab with sodium cation counterions placed between the surfactant headgroup and NaCl surface.

Prior to the interaction with water, the hybrid SDS/NaCl slabs were relaxed following an initial energy minimization with a 1 ns trajectory using the NAMD program. NAMD was developed by the Theoretical and Computational Biophysics Group in the Beckman Institute for Advanced Science and Technology at the University of Illinois at Urbana−Champaign.[35] The SDS molecules and Na^+ and Cl^- ions were described using the CHARMM27 lipid force field,[36] and the SHAKE algorithm constrained the lengths of covalent bonds to hydrogen.[37] Long-range electrostatic interactions were computed using the smooth particle mesh Ewald (PME) method,[38] and van der Waals interactions were truncated at a 12 Å cutoff distance. All simulations were run with a 1 fs time step and snapshots were saved at 1 ps intervals for detailed analysis. Langevin dynamics maintained a simulation temperature of 300 K.

Following the 1 ns relaxation of the SDS/NaCl slabs, 6 water molecules were added above each of the slabs and the simulations were run for an additional 1 ns. This amount of water is equivalent to the adsorption of ~0.04 ML of water, assuming a molecular packing density of 1×10^{15} molecules cm^{-2}.[39,40] The condition for water molecules sticking in the simulations is the water molecule coming within a specified distance from the NaCl surface and remaining there for the rest of the simulation. The TIP3P force field is used to model water as it is optimized for interactions of molecules with the CHARMM27 force field.[36] Density profiles of water, NaCl, and SDS were generated after these 1 ns trajectories.

In addition to the slab simulations, several runs with relaxation times between 0.1 and 1 ns were done with isolated NaCl/SDS particles built as shown in Figure 1. The goal of these simulations was to probe the behavior of SDS on corners and edges of the underlying NaCl crystal. MD simulations of water uptake by such isolated particles will be reported elsewhere.

The MD simulations reported here were performed to provide qualitative microscopic insight into the structure of the SDS−NaCl interface and the dynamics of water uptake on these surfaces as a function of SDS coverage. A number of previous studies have emphasized the importance of explicitly treating electronic polarization for an accurate description of the interfaces of aqueous ionic solutions.[41,42] In this work, nonpolarizable potentials were employed, in part because the SDS^- model chosen was refined for use with nonpolarizable water and counterions.[43] While we can expect slight changes in the interfacial composition in the SDS^-/NaCl(aq) systems,[42] the effects of neglecting polarizability in simulations of NaCl(s) are not well established. In any case, although certain atomic-scale structural features and the kinetics of water uptake might be slightly different if polarizable force fields were employed, we are confident that the simulations presented herein are sufficiently accurate to provide the qualitative insight for which they were intended.

***Ab Initio* Calculations.** Binding energies of $H_2O-(NaCl)_4$, sodium methyl sulfate (SMS)$-(NaCl)_4$, H_2O−SMS, and SMS$-H_2O-(NaCl)_4$ were calculated to explore the interactions occurring on the SDS/NaCl nanoparticle surface. SMS was chosen as a proxy for SDS and the $(NaCl)_4$ cluster was used to represent the NaCl particle in order to minimize computation time. The minimum energy structures were located using second-order Møller−Plesset[44−46] (MP2) perturbation theory with the cc-pVDZ basis set[47,48] (MP2/cc-pVDZ). Geometry optimizations[49−51] were carried out with the largest component of the analytic gradient[44,52] being smaller than 10^{-4} hartree/bohr. Minima were confirmed by an all-positive Hessian that was obtained by double differencing of analytic gradients.[53] The vibrational frequencies of H_2O were also calculated to quantitatively examine the nature of initially adsorbed water in these model systems. The reported values are scaled harmonic frequencies with a scaling factor of 0.95.[54] To benchmark the MP2 calculations, binding energies were calculated as single-point energies using the singles and doubles coupled cluster method, augmented by noniterative triples obtained perturbatively, CCSD(T), with the cc-pVTZ basis set (CCSD(T)/cc-pVTZ) using selected structures located on the MP2/cc-pVDZ potential energy surface.

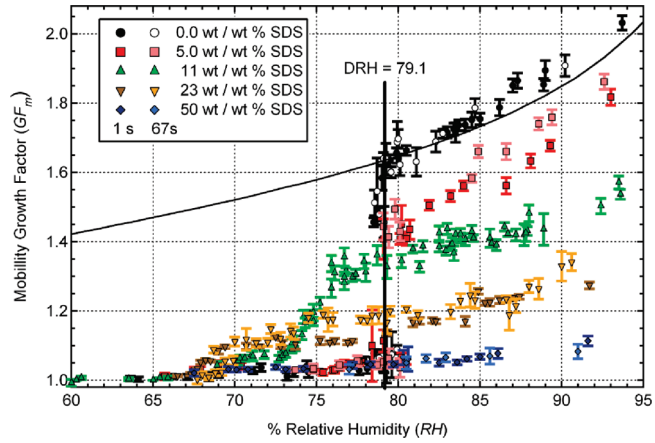

Figure 2. Hygroscopic growth curves of mobility equivalent diameter selected 14.0(±0.2) nm SDS/NaCl particles. The legend details wt/wt % of SDS/NaCl in solutions that were electrosprayed. The DRH of 14 nm NaCl particles from ref 10 is indicated by the thick solid line. The thin curve is a plot of the Köhler theory for 14 nm NaCl particles (eq 4). Labels 1 and 67 s refer to the time the nanoparticles were exposed to RH before being sized.

Results

Hygroscopic Growth of Pure NaCl and Hybrid SDS/NaCl Nanoparticles. Figure 2 shows the measured hygroscopic growth curves for size-selected 14.0(±0.2) nm particles containing variable amounts of SDS and NaCl. The legend details the composition of solutions that were electrosprayed (Table 2) as well as RH exposure time. The curve represents the Köhler theory expressed by eq 4 which takes into account the particle flow regime (free molecular),[5] the varying surface tension $\sigma_{aq}(w_t)$ with $NaCl_{aq}$ weight percent w_t,[28] as well as the empirically determined activity $a_w(w_t)$, and density $\rho_{aq}(w_t)$.[27]

For the pure NaCl nanoparticles, the present results corroborate the existing literature. The growth factors predicted by Köhler theory agree well with measured GF_m for the pure NaCl particles following deliquescence at high RH. The DRH value of 79.1% RH predicted from an empirical DRH-size relationship for NaCl developed by Biskos et al.[10] is also in good agreement with the observed DRH of 78.5% RH. Humidity exposure time does not make a difference for the hygroscopic growth or DRH determination of pure NaCl nanoparticles as the data points for the 1 and 67 s exposures are in excellent agreement. This indicates that any kinetic effect of water uptake and deliquescence occurs on time scales faster than the 1 s minimum duration of the RH exposure.

As the weight percent of SDS increases in the nanoparticles, GF_m are suppressed and the apparent location of DRH shifts to

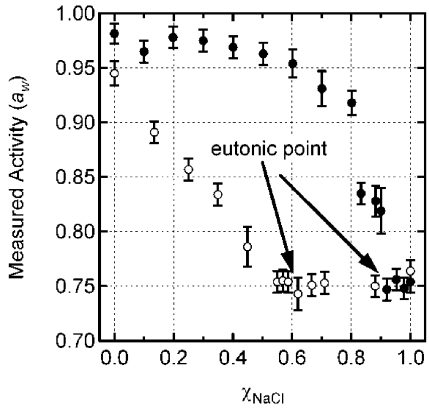

Figure 3. Measured water activities above saturated solutions of NaCl/Na_2SO_4 (open circles) and NaCl/SDS (filled circles) bulk solutions. Data are reported as a function of dry NaCl mole fraction (χ_{NaCl}) in the corresponding mixture of solids.

lower values of humidity in comparison to pure NaCl nanoparticles. Although growth factors are suppressed by the presence of SDS, the growth curves still have the same qualitative shape when compared to NaCl nanoparticles. Nanoparticles originating from the 5.0 wt/wt % SDS/NaCl solution display discontinuous deliquescence at the same RH value where pure NaCl nanoparticles deliquesce, 79.1(±1.0)% RH. Discontinuous deliquescence is not observed for nanoparticles generated from solutions containing more than 5.0 wt/wt % SDS. Nanoparticles from the 11 wt/wt % SDS/NaCl system deliquesce gradually between 73−77% RH and display a post-deliquescence growth curve that is qualitatively similar to pure NaCl nanoparticles, albeit at lower absolute GF_m. The nanoparticles from the 23 wt/wt % SDS/NaCl solution continue this trend but their growth curve has several unique features. For these nanoparticles, a fairly sharp growth region is observed between 68−71% RH, followed by a slower growth region until roughly 73% RH. Interestingly, there are indications of another growth factor increase between 73 and 75% RH but only for the nanoparticles exposed to RH for 67 s. After that the particles appear to grow steadily with RH with the rate characteristic of fully deliquesced droplets. The nanoparticles from the 50 wt/wt % SDS/NaCl solution have greatly suppressed growth and the onset of deliquescence is difficult to discern. Pure SDS nanoparticles do not take up any measurable amount of water at humidities between 5 and 95% RH ($GF_m < 1.02$), which is consistent with measurements from this laboratory on pure AOT nanoparticles.[5] Nanoparticles from the 50 wt/wt % SDS/NaCl solution definitively take up more water than neat SDS nanoparticles do in the 65−95% RH range.

The differences in the growth curves obtained with different RH exposure times (1, 7, and 67 s) are either undetectable or very small. The hygroscopic growth for SDS/NaCl nanoparticles as well as NaCl nanoparticles probably occur on time scales that are faster than experimentally measurable with a tandem nano-DMA setup. Indeed, deliquescence of NaCl has been theoretically shown to occur on time scales of microseconds to milliseconds.[55] The differences observed are likely due to the range of accuracy in measuring RH, which is ±1% between 0 and 90% RH and ±2% RH between 90 and 100% RH, and in measuring GF_m values (±0.02).

Water Vapor Activity over Bulk Mixtures. Figure 3 shows measured water vapor activity, a_w, as a function of dry NaCl mole fraction, χ_{NaCl}, in the NaCl/SDS (filled circles) and NaCl/Na_2SO_4 (open circles) mixtures submerged in H_2O. Since these are bulk measurements, the activity was calculated from eq 2.

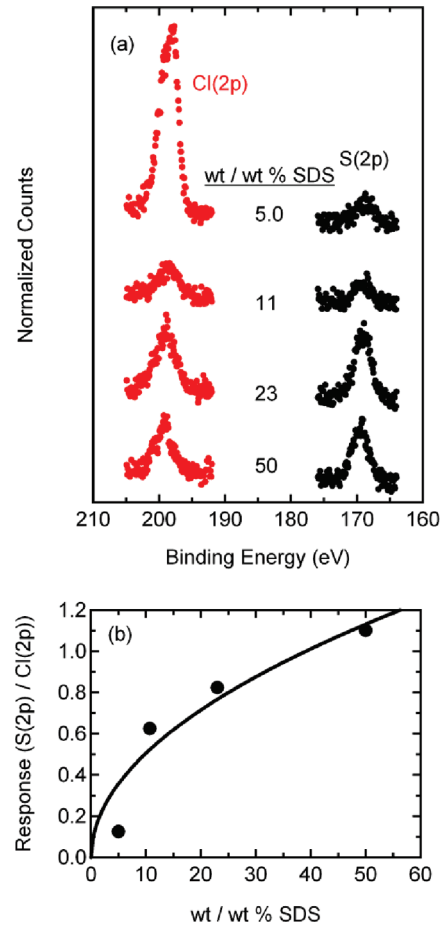

Figure 4. (a) Representative narrow scan spectra of S(2p) and Cl(2p) impacted SDS/NaCl nanoparticles on graphite; (b) the ratio of integrated peak areas for S(2p)/Cl(2p) plotted as a function of the SDS/NaCl wt/wt % in the electrosprayed solution.

There are no prior measurements for the NaCl/SDS mixture. The NaCl/Na_2SO_4 mixture, which was used for the validation of the measurements, has been examined previously.[56] The eutonic point of NaCl/Na_2SO_4, which corresponds to the composition of the mixture that minimizes water activity, 0.743(±0.015) (1σ deviation in repeat measurements) at χ_{NaCl} = 0.62, agrees well with previous studies.[56] Na_2SO_4 has a solubility of 21.9 wt % in water that is comparable with the NaCl solubility of 26.5 wt % at 298 K. SDS is less soluble in water (2.8 wt % in H_2O at 293 K) and appears to have a eutonic point at χ_{NaCl} = 0.92 corresponding to a measured activity of 0.747(±0.010). This is very close to the activity of a saturated NaCl solution of 0.764(±0.010) measured in this laboratory. Above the eutonic point, measured activities are analogous to a saturated NaCl solution where the NaCl solubility is weakly affected by the presence of SDS or Na_2SO_4. However, below the eutonic point, activity goes up monotonically. Here activity is equivalent to that of an undersaturated NaCl solution. Measured activities of pure SDS and Na_2SO_4 solutions at χ_{NaCl} = 0 are close to unity, 0.982(±0.010) and 0.945(±0.011), respectively. As water vapor suppression is a colligative property, these measurements indicate that high concentrations of SDS reduce the apparent NaCl solubility.

Characterization of SDS/NaCl Nanoparticles. Figure 4a shows representative narrow scan XP spectra of S(2p) and Cl(2p) photoelectrons from the various compositions of SDS/NaCl nanoparticles prepared under conditions listed in Table 2. The nanoparticles analyzed by XPS were not size selected

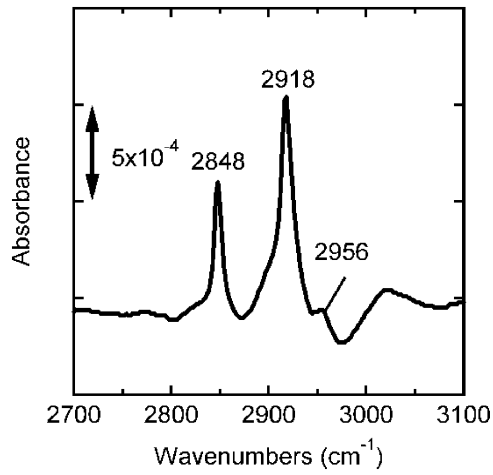

Figure 5. Transmission FTIR spectra of impacted 23 wt/wt % SDS/NaCl nanoparticles on a ZnSe window in the CH-stretching vibration region.

for this measurement; the full nanoparticle size distribution of each composition is impacted for analysis. Spectral features of S(2p), Cl(2p), O(1s), and Na(1s) did not change significantly after several exposures totaling 30 min and thus are not affected by beam damage. Differences in the absolute peak areas of the S(2p) and Cl(2p) are attributed to difficulties in positioning the nanoparticle deposition ring directly under the optimum sampling position for the electron energy analyzer. To avoid these problems, only relative intensities are used in the analysis. It should be noted the S(2p)/Cl(2p) ratio is not an absolute measure of the relative SDS content in nanoparticles because the effective XPS probe depth depends on the particle morphology, which is unknown a priori.

Figure 4b shows the S(2p)/Cl(2p) ratio of integrated peak areas as a function of solution composition from which nanoparticles are generated. Nanoparticles from different solutions display markedly different S(2p)/Cl(2p) ratios, which increase with the amount of SDS. The largest increase is observed in going from the 5.0 to 11 wt/wt % SDS. As the fraction of SDS increases further (23 and 50 wt/wt % SDS), the S(2p)/Cl(2p) ratio shows signs of saturation. Table 2 shows that the size of the nanoparticles from the 5.0 and 11 wt/wt % SDS solutions is similar, while the impacted sizes for the nanoparticles from the 23 and 50 wt/wt % SDS/NaCl systems are larger. This size difference may affect both the average composition of nanoparticles generated by the electrospray source and the relative XPS response. It is assumed the effect of the impacted particle size on the relative S(2p)/Cl(2p) XPS response is minimal, and the S(2p)/Cl(2p) measurement is positively correlated with the relative amount of SDS and NaCl on the surface of the particles.

Figure 5 shows an FTIR spectrum of nanoparticles from the 23 wt/wt % SDS system impacted on a ZnSe window without size selection. The CH-stretching region (2700−3100 cm^{-1}) is plotted to show characteristic vibrations of the aliphatic moiety of SDS. The peaks at 2848, 2918, and 2956 cm^{-1} are attributed to the symmetric $-CH_2-$ stretch (ν_{sym}), the asymmetric $-CH_2-$ stretch (ν_{as}), and the asymmetric $-CH_3$ stretch, respectively.[57] Bands associated with the $-O-SO_3^-Na^+$ moiety were detectible at lower frequencies; however, the signal-to-noise ratio was poor due to the small amount of material analyzed.

Figure 6 shows representative AFM images of 23 wt/wt % SDS/NaCl nanoparticles impacted on HOPG. For these measurements, the particles were size selected (21 nm, GSD = 1.05) prior to impaction. These AFM images reveal that particles

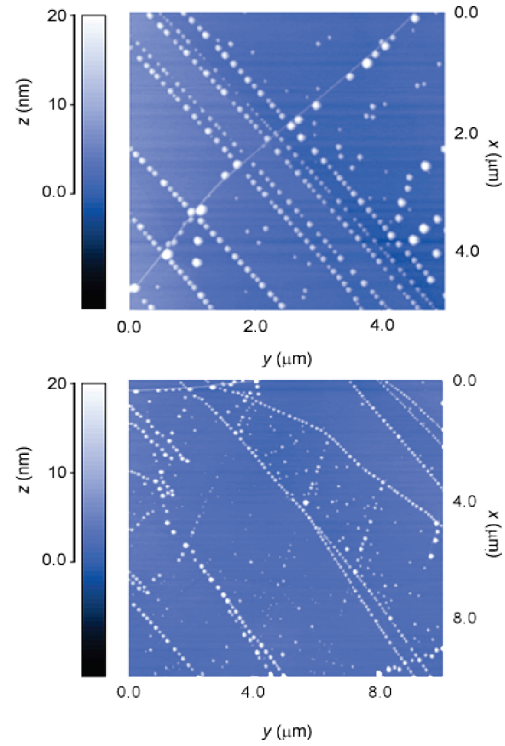

Figure 6. AFM images of 21 nm mobility equivalent diameter 23 wt/wt % SDS/NaCl nanoparticles on HOPG at different resolutions. Particles preferentially align along the HOPG step edges. The measured particle heights are in good agreement with the mobility equivalent diameter.

preferentially align with the graphite step edges. Line scan analysis of the observed particle heights (not shown) indicates the size-selected mobility diameter was consistent with the AFM-imaged diameter. Despite the size selection, some images contained a number of very small particles (<3 nm). Such small particles are not efficiently screened by the DMA due to diffusional limitations. Presence of these particles does not affect the results of the hygroscopic growth measurements as the condensation particle counter is very insensitive to particles in this size range.

Molecular Dynamics Simulations of SDS/NaCl Slabs. Figure 7a shows MD simulation snapshots of different SDS/NaCl slabs (Θ_{SDS} = 0.25, 0.40, 0.60, and 0.80 ML) on a crystalline NaCl. The side view makes it clear that, as Θ_{SDS} increases, the alkyl chains in SDS become more ordered and the apparent thickness of the SDS layer increases. The top view reveals that at low Θ_{SDS} values, bare patches of NaCl are exposed to the gas-phase and this accessibility decreases as Θ_{SDS} increases. The ability of water to stick to the SDS/NaCl slabs is correlated with the fraction of exposed NaCl and anticorrelated with Θ_{SDS}. After 1 ns of interaction with 6 simulated water vapor molecules and a relaxed SDS/NaCl slab corresponding to Θ_{SDS} = 1.0 ML (not shown in Figure 7), no water molecules penetrate the SDS layer and stick to the hydrophilic NaCl surface. As Θ_{SDS} decreases, the water molecule sticking probability increases as the arrow in Figure 7a indicates. For example, all 6 water molecules quickly end up on the NaCl surface during a simulation of the Θ_{SDS} = 0.25 ML slab.

Figure 7b shows a MD simulation snapshot of an SDS/NaCl slab (Θ_{SDS} = 0.60 ML) on an aqueous NaCl solution. The side view reveals that both the SDS−core interface and the SDS alkyl chains are more disordered when the core is a solution as opposed to a crystal. The top view reveals bare

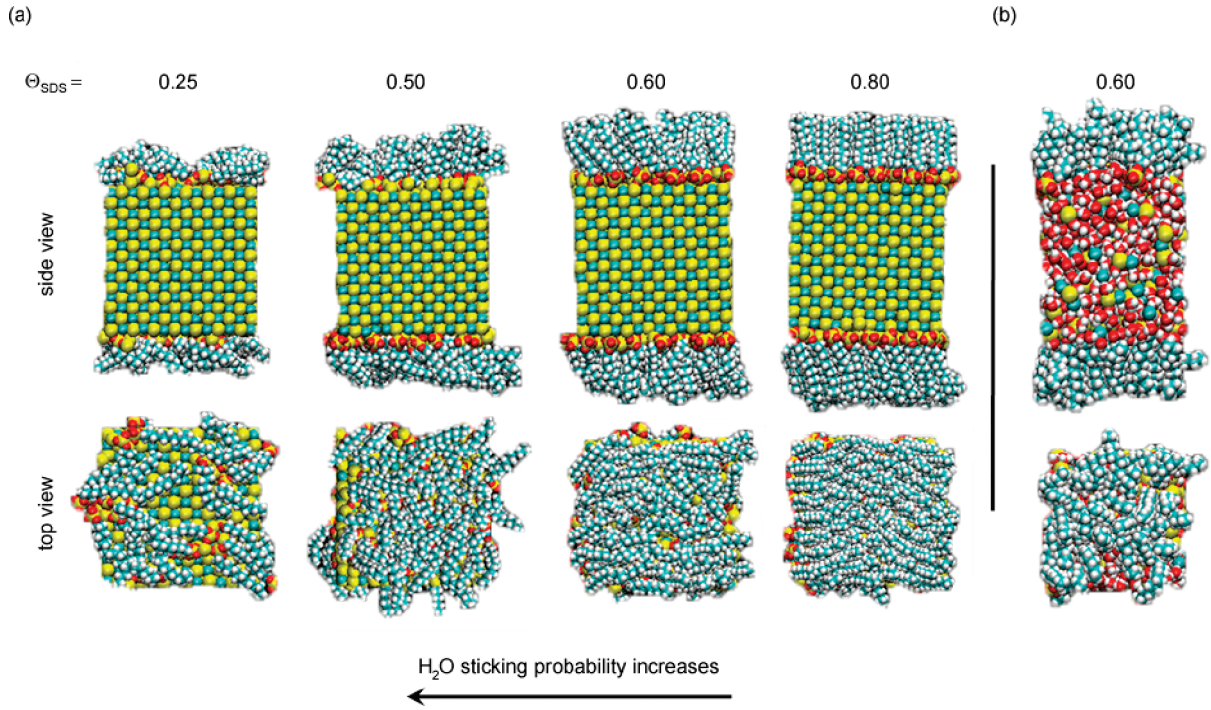

Figure 7. MD simulation snapshots of varying SDS coverage (Θ_{SDS}) on SDS/NaCl slabs on (a) crystalline NaCl core and (b) aqueous NaCl solution core. As the SDS coverage decreases the H_2O sticking probability increases. Coloring scheme: O, red; S and Na^+, yellow; C and Cl^-, cyan; H, white.

patches of solution exposed to the MD simulation vapor phase, which is similar to the $\Theta_{SDS} = 0.60$ ML simulation on a crystalline core. In contrast to the crystalline core trajectory, all 6 water molecules quickly entered the solution core and remained in the condensed phase for the remainder of the simulation time. This difference is attributed to the greater degree of disorder in the SDS shell on the aqueous core.

***Ab Initio* Structures and Binding Energies.** The located minimum energy structures and corresponding binding energies of selected complexes are shown in Figure 8, where oxygen is colored red, hydrogen is white, sodium cation is black, chloride anion is green, and carbon is also black. The optimized structures of H_2O, SMS, and $(NaCl)_4$ are given in Figure 8, a, b, and c, respectively. A number of possible structures of SMS bound to $(NaCl)_4$ were found and three representative structures are shown in Figure 8d−f. Binding energies were calculated as a difference in energies of the bound with respect to free species. The weakest binding of -12.1 kcal mol^{-1} was found for cases when the methyl group in SMS is interacting with $(NaCl)_4$ as seen in Figure 8d. As expected, the strongest binding energies were found when the polar headgroup in SMS is interacting with $(NaCl)_4$. Binding energies were in range of -31.9 to -34.7 kcal mol^{-1} for these complexes. Shown are two representative structures with binding energies of -34.7 kcal mol^{-1} in Figure 8e and -32.5 kcal mol^{-1} in Figure 8f. A large distortion of the $(NaCl)_4$ lattice due to SMS binding is observed in some of the complexes. Such lattice distortions are expected to be much less pronounced in the extended lattice of the NaCl nanoparticle. The binding energy of adsorption to an extended NaCl surface may therefore be different from the binding energies calculated for the model systems presented in Figure 8. However, it is clear that SDS should form a very strong ionic bond to NaCl, and these bonds are expected to be stable at ambient temperatures.

Three representative complexes between H_2O and $(NaCl)_4$, SMS, and SMS−$(NaCl)_4$ are shown in Figure 8, g, h, and i, respectively. Only one preferred configuration was found for H_2O binding to $(NaCl)_4$. In this complex, the oxygen atom in H_2O interacts with a sodium cation in $(NaCl)_4$. In addition, a hydrogen atom in H_2O is hydrogen bonded to the adjacent chloride ion. The binding energy of this complex (Figure 8g) is -20.2 kcal mol^{-1} at the MP2/cc-pVDZ level of theory and -14.8 kcal mol^{-1} at the CCSD(T)/cc-pVTZ level of theory. SMS binds H_2O in several possible configurations involving different oxygen atoms of SMS's polar headgroup and one of the hydrogen atoms of H_2O. Aside from the hydrogen bond being present in all of the located minimum energy structures, another common motif is binding of the oxygen atom from H_2O to the sodium cation in SMS. The calculated binding energy of H_2O to SMS ranges from -23.2 to -25.6 kcal mol^{-1} (MP2/cc-pVDZ). Shown in Figure 8h is the complex with the strongest binding energy of -25.6 kcal mol^{-1} at the MP2/cc-pVDZ level of theory and -18.4 kcal mol^{-1} at the CCSD(T)/cc-pVTZ level of theory.

Most relevant to this work is the structure that involves binding of both H_2O and SMS to $(NaCl)_4$, Figure 8i. In this structure, the oxygen from H_2O interacts with the sodium cation from SMS, while both hydrogen atoms from H_2O are hydrogen bonded, one to the S−O−C oxygen from SMS and the other to a chloride ion in $(NaCl)_4$. The overall binding energy for this structure (-61.5 kcal mol^{-1}) exceeds the sum of binding energies of H_2O and SMS, suggesting strong cooperation of their interactions.

Calculated vibrational frequencies of H_2O in selected structures are reported in Table 3. The frequencies of the symmetric and asymmetric stretches decrease relative to gas-phase H_2O (Figure 8a) when H_2O is bound to $(NaCl)_4$ (Figure 8g), SMS (Figure 8h), or both (Figure 8i). This is consistent with ordered thin films of water on NaCl surfaces under ambient conditions.[1] For water interacting with structures that

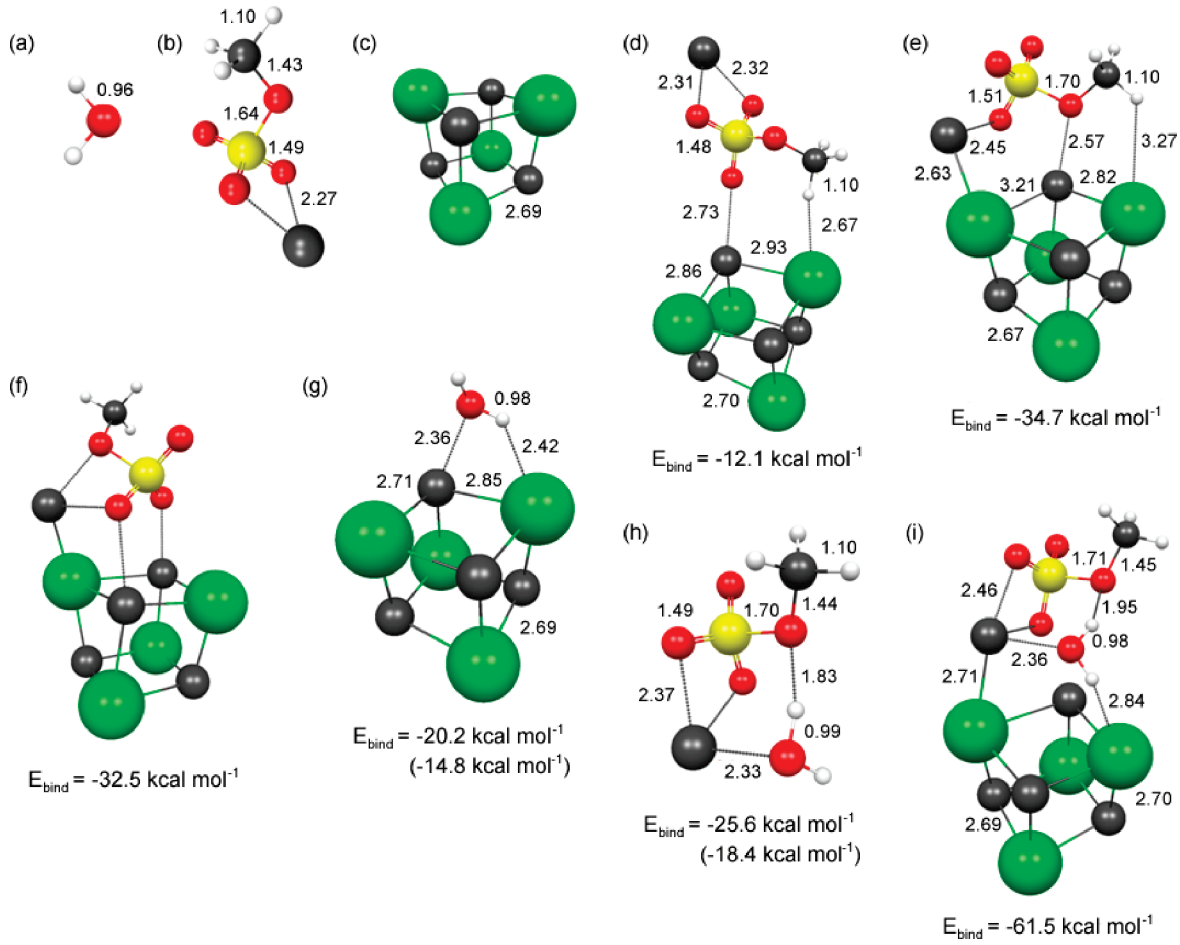

Figure 8. Located energy minima for (a) H_2O; (b) sodium methyl sulfate (SMS); (c) $(NaCl)_4$; (d−f) SMS−$(NaCl)_4$; (g) H_2O−$(NaCl)_4$; (h) H_2O−SMS; and (i) SMS−H_2O−$(NaCl)_4$. Bond lengths are in angstroms (1 Å = 0.1 nm). The binding energies (E_{bind}) correspond to the MP2/cc-pVDZ level of theory. Binding energies at the CCSD(T)/cc-pVTZ level of theory are shown in parentheses for selected structures.

TABLE 3: Calculated Shifts in the Frequencies of H_2O Vibrations in Selected Complexes Relative to Free H_2O

structure[a]	ν_{as} (cm^{-1})	ν_{sym} (cm^{-1})	ν_{bend} (cm^{-1})
H_2O (a)	3772[b]	3659	1594
H_2O−$(NaCl)_4$ (g)	−57	−111	−6
H_2O−SMS (h)	−65	−281	+32
SMS−H_2O−$(NaCl)_4$ (i)	−172	−160	+33

[a] Selected structures from Figure 8. [b] The top row contains calculated frequencies for free H_2O; the remaining rows are frequency shifts with respect to free H_2O.

include SMS (Figure 8h,i) the H_2O bending mode increases relative to the gas phase, likely due to ring structures resulting from hydrogen bonds.

Discussion

Predeliquescent Wetting of NaCl and SDS/NaCl Nanoparticles. Crystalline NaCl is known to adsorb 3.5−4.0 ML of water at humidities just below 75.4% RH at room temperature and pressure.[1,3,4] For a 100 nm particle this would translate in a GF_m of ∼1.01. Quantification of ML coverage on large (>100 nm) NaCl particles is therefore difficult in a tandem DMA experiment. On the other hand, the GF_m of a 10 nm particle with 3.5−4.0 ML is ∼1.10, which is well above the minimum detectable growth under experimental conditions employed in this work ($GF_m = 1.00 \pm 0.02$). Here we take advantage of the tandem DMA approach to learn about predeliquescent water uptake on SDS/NaCl particles.

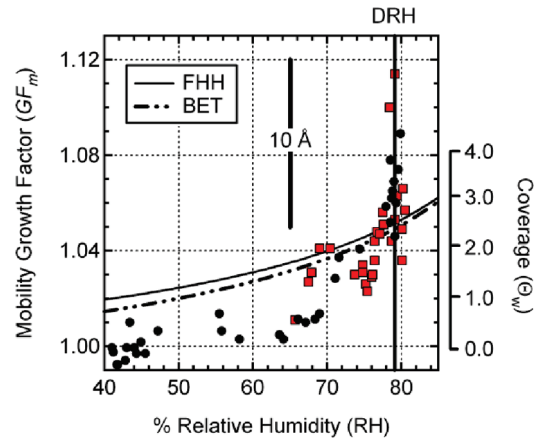

Figure 9. Standard adsorption isotherms compared to experimental data for 14 nm NaCl (black circles) and 5.0 wt/wt % SDS/NaCl (red squares) particles.

Figure 9 shows the same measured GF_m vs RH data presented in Figure 2 with special attention given to the predeliquescence region. Error bars have been omitted to reduce congestion. The 10 Å scale bar demonstrates the sensitivity to molecular scale growth when examining 14 nm particles in a tandem-nano DMA experiment. The solid line represents the Frenkel−Halsey−Hill (FHH) water adsorption isotherm[58,59] and the hatched line represents the Brunauer−Emmett−Teller (BET) isotherm.[58,59] The DRH of 14 nm NaCl particles[10] is also indicated by the thick solid line. For convenience, the isotherms are converted

into growth space (GF_m vs RH) and include a correction for the Kelvin effect $C_K(\sigma_{aq},d_m)$ as well as a shape correction $A(Kn,\chi_v)$.

Isotherms are converted into growth space by use of the definition of a water coverage layer ($\Theta_w = S_w/S_{NaCl}$)[1] and plugging the appropriate isotherm equation $\Theta_w(S)$ into eq 6. S_w is the surface density (molecules cm^{-2}) of water calculated from measured GF_m and S_{NaCl} is the surface density of ion pairs for the (001) face (6.4×10^{14} cm^{-2}).[60] A derivation of S_w is available in a previous publication.[5] In eq 6, the envelope equivalent diameter is $d_e(0) = 12.6$ nm and the shape correction parameter is $A(Kn,\chi_v) = 0.898$. Appropriate FHH ($A = 0.96$, $B = 1$) and BET ($c = 1.5$) constants are used for water adsorption on the NaCl(001) surface.[1,8,58,59] The bulk density of water (997.1 kg m^{-3}) is converted to the molecular units (33 molecules nm^{-3}) for ρ_w^{molec}.

$$GF_m(RH) = \left[\left(\frac{6S_{NaCl}A^3(Kn,\chi_v)}{\rho_w^{molec}d_e(0)}\right)\Theta_w(S) + 1\right]^{1/3} \quad (6)$$

As can be seen in Figure 9, there is fair agreement between the measured GF_m of NaCl and 5 wt/wt % SDS/NaCl 14 nm particles and eq 6 in the region corresponding to 1.5 ML < Θ_w < 3.0 ML (1.02 < GF_m < 1.06) occurring at roughly 70% RH. At the lower values of RH, the experimental growth factors are reproducibly lower than the ones predicted from the isotherms. In fact, the measured GF_m of NaCl are actually *smaller than 1.00* near ~40% RH. This is attributed to dynamic reshaping of NaCl nanoparticles upon interaction with initially adsorbed surface water at $\Theta_w \ll 1.0$ ML.[61,62] This restructuring of the NaCl nanocrystal changes its shape toward sphericity thus reducing its mobility equivalent diameter. The data points above $\Theta_w > 3.0$ ML ($GF_m > 1.06$) for both NaCl and 5.0 wt/wt % SDS/NaCl nanoparticles are from mobility histograms that contained two mode diameters (see discussion below). Consequently, the error in the Θ_w calculation is large in this region due to fluctuations of particles coexisting in a wetted crystalline state and dissolved droplet state.

Inversion of eq 6 at the DRH of 14 nm NaCl (79.1% RH)[10] results in a predicted coverage of 2.4 ML of adsorbed surface water according to the FHH isotherm and 2.3 ML according to the BET isotherm. Similar inversion that starts with the measured GF_m value (at 1 and 67 s RH exposure) reveals an estimated surface coverage of $\Theta_w = 3.1(\pm 0.5)$ ML (propagation of 2σ error in measured GF_m) of adsorbed surface water on 14 nm NaCl particles. Note that 79.1% RH above a 14 nm particle surface is equivalent, after accounting for the Kelvin effect (eq 4), to 67.3% RH (20.0 mbar at 297K) above a bulk NaCl crystalline surface, which has roughly 3 ML of adsorbed surface water.[1] It can be concluded that the thickness of the water film on predeliquesced NaCl particle is quantitatively consistent with measurements done on bulk NaCl after properly accounting for the Kelvin effect.

A similar analysis for 5.0 wt/wt % SDS/NaCl nanoparticles reveals an estimated water surface coverage of $\Theta_w = 3.1(\pm 0.5)$ ML, which is identical to the coverage on pure NaCl nanoparticles within experimental uncertainties. This suggests that a submonolayer to a full monolayer coverage of SDS (estimation of the SDS coverage is detailed below) does not greatly interfere with predeliquescent water uptake. This adsorbed water is likely to sit on the surface of the NaCl crystal, with SDS floating on the surface in the form of a soapy film. Similar conclusions about the morphology of wetted but not fully deliquesced NaCl/SDS particles were reached in a recent experimental study that relied on a probe molecule spectroscopy technique.[18]

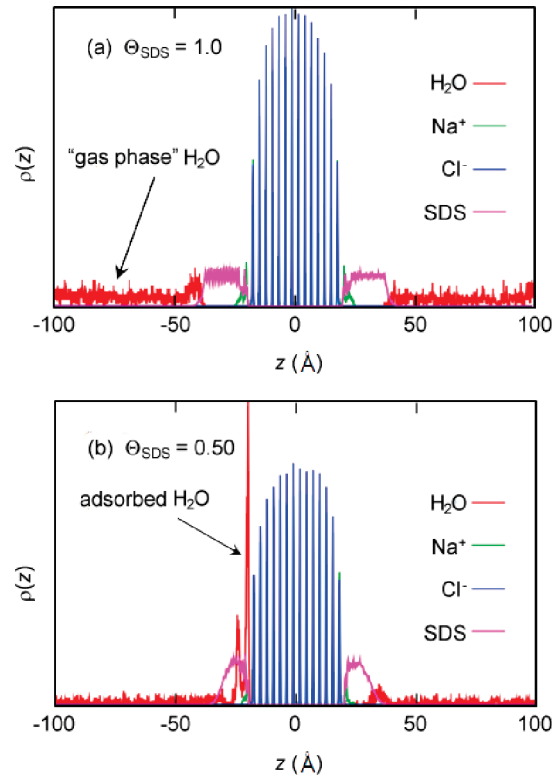

Figure 10. Density profiles (arbitrary units) of H_2O, Na^+, Cl^-, and SDS after 1 ns interaction with 6 water molecules. The full coverage slab ($\Theta_{SDS} = 1.0$) is presented in panel (a) and the half-coverage slab ($\Theta_{SDS} = 0.50$) is presented in panel (b).

Molecular Dynamics Simulations of SDS/NaCl Slabs and Particles. According to the MD simulations results presented in Figure 7a, bare patches of NaCl facilitate adsorption of water molecules to the NaCl surface. Figure 10 shows density profiles of the full coverage slab ($\Theta_{SDS} = 1.0$ ML) and half coverage ($\Theta_{SDS} = 0.50$ ML) slab after 1 ns of interaction with 6 water vapor molecules. As can be seen in Figure 10a, water molecules are unable to penetrate the full SDS layer and remain in the "gas phase," which in the simulation is a vacuum. In Figure 10b, 3 water molecules are adsorbed to the SDS/NaCl interface, one is interacting with a terminal methyl group and the remaining waters are still in the "gas phase." The initial adsorption of water molecules on nanoparticles with a moderate SDS coverage should therefore occur on bare NaCl patches. Water molecules are likely to end up in the vicinity of a polar SDS headgroup because of their ability to form a hydrogen bond to both Cl^- and the SMS headgroup as depicted in the *ab initio* structure presented in Figure 8i.

In addition to modeling slabs of NaCl coated with SDS, we also conducted several MD simulations on isolated SDS/NaCl particles with the goal of visualizing the behavior of SDS on the edges of the NaCl nanocrystal. Figure 1 provides an example of such a simulation after 100 ps relaxation time. These simulations predict a significant degree of distortion of the NaCl structure by SDS near the edges and corners of the NaCl crystal. These sites are the least protected from water by the alkyl tails of SDS, and therefore represent the most likely sites for the initial H_2O adsorption. From there, H_2O can percolate in between NaCl and SDS, and eventually deliquesce the NaCl crystal.

The direct comparison between the MD simulations and the experiment is not straightforward. The experiment gauges the

size of the SDS/NaCl particle in equilibrium with water vapor; it provides only a crude upper limit of 1 s for the time scales involved in the initial water uptake and deliquescence. The MD simulation demonstrates that SDS introduces a sizable kinetic barrier to the initial water uptake; a significant reduction in the amount of adsorbed water is observed on the 1 ns time scale of the simulation. Despite these limitations, the MD simulations presented here make it possible to visualize the processes involved in the initial adsorption of water to SDS/NaCl surfaces on a molecular level. Future MD simulations will explicitly probe interactions of "gas-phase" water molecules with a structure similar to that presented in Figure 1 or that in Figure 8i.

Structure of SDS/NaCl Nanoparticles Inferred from Their Hygroscopic Growth. Hygroscopic growth of SDS/NaCl nanoparticles can teach us about the composition and morphology of SDS/NaCl nanoparticles produced in the electrospray process. SDS and NaCl are likely to phase-segregate during the primary and progeny droplet evaporation in the electrospray source. Once the evaporation stage is complete, nanoparticles should have a NaCl crystalline core decorated by a film of SDS molecules and possibly some residual water remaining in between SDS and NaCl (the evidence for the residual water comes from very long drying times for the SDS/NaCl particles in the FTIR spectrometer). Zelenyuk et al.[21] reported residual solvent in SDS/NaCl particles (>100 nm) after diffusion drying and its presence in SDS/NaCl particles could lead to a variety of different SDS meso-phases (i.e., liquid crystals, micelles, etc.) which will contribute to markedly different SDS densities.[21] Assuming core−shell morphology, the submonolayer SDS film on NaCl is likely to have the $-O-SO_3^-Na^+$ headgroup of SDS pointing to the NaCl surface in an inverted micelle like orientation. This is consistent with the morphology of 70−100 nm SDS/NaCl particles deduced by Woods et al.[18] from probe molecule spectroscopy. The MD simulations and the *ab initio* structures presented in Figure 8d−f also indicate there is a strong energetic benefit for SDS to exist in this morphology on the NaCl nanoparticle surface.

When the amount of SDS exceeds the amount needed for one monolayer, the excess SDS can either accumulate in a "blob" attached to the particle or coat the surface more uniformly with a multilayer film of SDS. The effective thickness of the SDS coating should increase with the SDS weight fraction in the solutions that were electrosprayed. This appears to be a good initial assumption as GF_m are monotonically suppressed in growth curves (Figure 2) as the weight percent of SDS increases. The relative S(2p)/Cl(2p) XPS signal also grows with the SDS weight fraction (Figure 4); however, converting the measured S(2p)/Cl(2p) ratio into the absolute SDS wt % is not straightforward for a number of reasons (see below). The actual thickness of the SDS film can be estimated using a simple model,[5] which assumes core−shell morphology and the volume of each component is represented by bulk densities (ρ_{NaCl} and ρ_{SDS}) and amounts of NaCl and SDS. Equation 7 shows how the core NaCl diameter (d_{NaCl}) is calculated, where w_t is NaCl weight percent and d_m is the overall particle diameter. The effective SDS film thickness (Δ_{SDS}) is then calculated as $(d_m - d_{NaCl})/2$.

$$d_{NaCl} = \left(\frac{w_t \rho_{SDS} {d_m}^3}{\rho_{NaCl} - (\rho_{NaCl} - \rho_{SDS}) w_t} \right)^{1/3} \quad (7)$$

We would like to emphasize, however, that these calculations are rather approximate as the density and weight fraction of the surfactant layer is uncertain. For example, Tsai et al.[63] studied Au nanoparticles (10−60 nm) functionalized with alkanethiol self-assembled monolayers (SAMs) and showed the organic coating was quite "soft". The actual thickness of the organic coating, which was deduced from temperature-programmed desorption and mobility diameter measurements, was found to be smaller than expected from purely geometric considerations.[63]

The ZSR model (eq 8) can be used to estimate the relative volume fractions, ε_{SDS} and ε_{NaCl}, of SDS and NaCl in the SDS/NaCl nanoparticles.

$$\begin{aligned} GF^3_{particle} &= \varepsilon_{NaCl} GF^3_{NaCl} + \varepsilon_{SDS} GF^3_{SDS} \\ GF^3_{particle} &\approx 1 + \varepsilon_{NaCl} (GF^3_{NaCl} - 1) \end{aligned} \quad (8)$$

Pure SDS nanoparticles do not adsorb any measurable amount of water in the range of 5−95% RH; therefore, it is assumed the ZSR model only depends on growth factor for NaCl (GF_{NaCl}). The right-hand side of eq 4 is substituted for GF_{NaCl} in eq 8 and the NaCl volume fractions (ε_{NaCl}) expected from electrosprayed solutions (Table 2) are used as the initial guesses. ε_{NaCl} is then used as an adjustable parameter to get the best agreement between the ZSR predictions and experimental observations. Figure 11 shows the results for 14 nm (17 nm for pure SDS) particles composed of (b) 5.0 wt/wt % SDS/NaCl; (c) 11 wt/wt % SDS/NaCl; (d) 23 wt/wt % SDS/NaCl; (e) 50 wt/wt % SDS/NaCl; (f) pure SDS. The ZSR model clearly fails with the assumption that the nanoparticle composition is identical to that of the electrosprayed solutions. The agreement improves significantly if one allows for an *enhancement* of SDS relative to NaCl in the electrosprayed droplets. The dotted lines in Figure 11 represent optimized dry NaCl volume fractions based on GF_m measurements of SDS/NaCl nanoparticles. There is excellent agreement in the shape of predicted GF_m in the parametrized ZSR model with measured GF_m. Table 4 summarizes the results of this analysis, where the SDS weight percent calculated from the ZSR model is compared to the composition of the initial solution.

The ZSR model predicts significant SDS enhancement in nanoparticles relative to the solutions from which they were electrosprayed. In our previous experiments with the AOT/NaCl particles,[5] an AOT enhancement was also observed, however, not to the extent as for the SDS/NaCl particles. These differences likely reflect stronger surfactant properties of SDS relative to AOT. The observation of surfactant enhancement in nanoparticles in this work and previously[5] is consistent with other studies involving electrospraying surface active materials. Tang and Smith[64] observed smaller satellite and progeny droplets generated by the spray formation and asymmetric fission processes to be enhanced in surfactants SDS and Flurad carbon (FC-171, $C_8F_{17}SO_2N(C_2H_4O)_7CH_3$), a nonionic liquid surfactant. It is uncertain which generation of droplet fission in the electrospray process the SDS/NaCl nanoparticles originated from. It was empirically found that the nanoparticle size characteristics changed dramatically when the electrospray protocols presented in Table 2 were altered. Specifically, variance of the electrospray distance l_s had the largest effect on the size distribution as well as measured hygroscopic properties of the resulting SDS/NaCl particles. This suggests different generations of droplets could likely have a different SDS content, which is consistent with Tang and Smith's observations of surfactant enhancement in the progeny droplets. It should be noted the electrospray

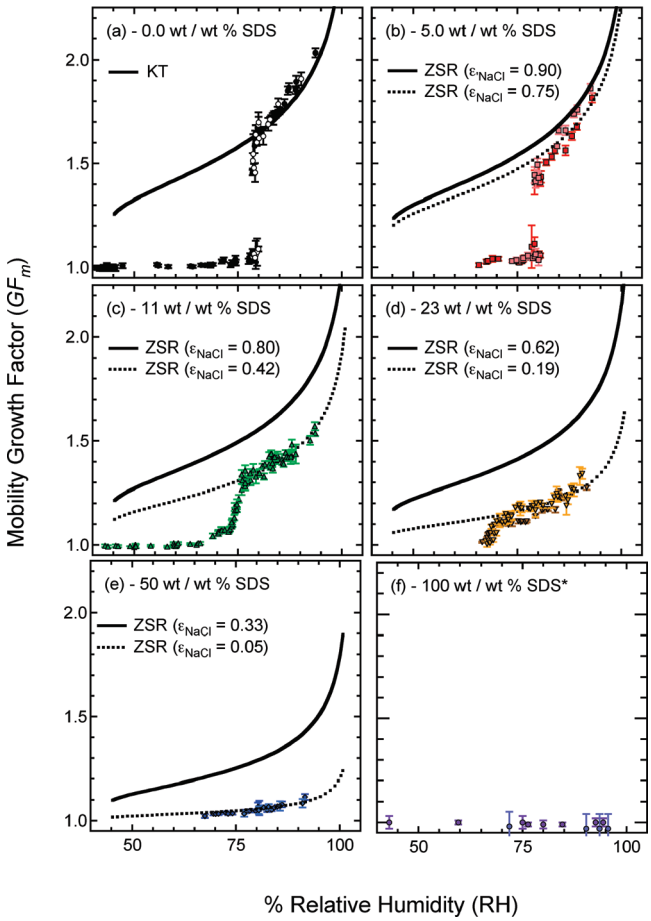

Figure 11. Predictions of Köhler theory (KT, eq 4) and the ZSR model (eq 8) compared to the experimental data for 14 nm (a) NaCl, (b−e) SDS/NaCl, and (f) 17 nm pure SDS particles. Solid lines represent predictions that use NaCl volume fractions (ε_{NaCl}) expected from bulk solutions. Dotted lines represent ZSR model results with the NaCl volume fractions adjusted to fit the GF_m measurements. Both 1 s and 67 s RH exposure data sets are plotted (see legend in Figure 2).

apparatus used in this work is custom built and without detailed knowledge of the electric field characteristics, it is difficult to compare our apparatus to commercial electrospray particle generators. Nevertheless, we can expect that other electrospray particle generators should similarly produce particles that are enhanced in the relative amount of surface active species.[65]

The effective SDS coverage for $\Theta_{SDS} \leq 1.0$ ML can be calculated from the assumed values of ε_{NaCl} (either from the solution composition or from the ZSR fits).[5] This analysis reveals for the 5.0 wt/wt % SDS/NaCl nanoparticles $\Theta_{SDS} = 0.4$ ML assuming the composition is that of the electrosprayed solution. The parametrized ZSR model composition of these nanoparticles predicts that the actual SDS fraction in these particles is roughly 14 wt/wt %, translating to $\Theta_{SDS} = 1.0$ ML. The true SDS coverage is likely to be in between these two values. The adsorption isotherm analysis presented above shows that water forms a film of the same thickness on pure NaCl and on the 5.0 wt/wt % SDS/NaCl particles. This suggests that SDS does not greatly interfere with NaCl−H_2O interactions at $\Theta_{SDS} \leq 1.0$ ML. The thickness of the SDS layer for the remaining SDS/NaCl compositions is expected to exceed 1.0 ML based on the parametrized ZSR model results.

Deliquescence in SDS/NaCl Nanoparticles. In this paper, "discontinuous deliquescence" refers to the coexistence of two distinct phases, wetted crystalline and aqueous droplet, over a very narrow range of RH (±1% RH). This coexistence manifests itself in a bimodal mobility equivalent diameter distribution in the vicinity of the DRH values, with the lower diameter corresponding to particles that have not yet deliquesced and the larger diameter corresponding to the aqueous droplets.[10] Once RH increases slightly the dry phase disappears in a discontinuous manner, and only the aqueous particles remain. In contrast, "gradual deliquescence" refers to a smooth evolution in the particle size distribution over the range of RH corresponding to the particle deliquescence.

Whereas pure NaCl nanoparticles undergo discontinuous deliquesce, presence of sufficient amounts of SDS or AOT (sodium bis(2-ethylhexyl) sulfosuccinate)[5] makes the deliquescence more gradual. Discontinuous deliquescence is still observed with 5.0 wt/wt % SDS/NaCl nanoparticles at the same RH as pure NaCl nanoparticles. Per the above discussion these particles are coated with a submonolayer of SDS. Discontinuous deliquescence is no longer observed in particles with higher SDS weight fractions, which correspond to SDS coverage in excess of a monolayer.

The end point of a gradual deliquescence transition can be clearly recognized when viewing the data plotted with the parametrized ZSR models. The ZSR model describes an aqueous phase and, therefore, a phase transition from crystalline to aqueous phase can be viewed as complete when the growth curve converges onto the respective ZSR model predictions. The 11 and 23 wt/wt % SDS/NaCl data sets converge to their respective ZSR models over several %RH units, with particles achieving fully deliquesced states at 76.8% RH and 70.7% RH, respectively. Only one mode diameter is observed in mobility histograms across the entire RH range studied for both of these compositions. It is therefore concluded that the 11 and 23 wt/wt % SDS/NaCl nanoparticles are partially dissolved droplets during their observed gradual deliquescent growth. It is difficult to discern a deliquescence-like transition in the 50 wt/wt % SDS/NaCl nanoparticle growth curves. ZSR analysis reveals the NaCl volume fraction of these nanoparticles to be 0.05; therefore, it is not surprising the nanoparticles barely grow, even at high RH values.

SDS/NaCl Nanoparticle Activity vs NaCl/SDS Bulk Mixture Activity. Soluble multicomponent particles display mutual deliquescence at the eutonic point (χ_{solute}, a_w) of the corresponding bulk mixture.[13] In Figure 3, the eutonic composition of NaCl/SDS occurs at $\chi_{NaCl} = 0.92$. At NaCl mole fractions exceeding this composition, the activity is nearly the same (±1% RH) as that of a pure NaCl solution. SDS/NaCl nanoparticles studied in this work should therefore display mutual deliquescence in the same vicinity (±1% RH) as pure NaCl nanoparticles at compositions of $0.92 \leq \chi_{NaCl} < 1.00$. Table 4 indicates that, if the composition of the nanoparticles were the same as the electrosprayed solutions, then the 5.0, 11, and 23 wt/wt % SDS/NaCl nanoparticles would have displayed mutual deliquescence at roughly the deliquescence point of pure NaCl nanoparticles. This is not the case as only the 5.0 wt/wt % SDS/NaCl nanoparticles displayed mutual deliquescence at the NaCl nanoparticle deliquescence point. This observation is more consistent with compositions from the ZSR model, which predicts that 5.0 wt/wt % SDS/NaCl nanoparticle is the only composition satisfying the condition $0.92 \leq \chi_{NaCl} < 1.00$.

The observations for the mutual deliquescence of the bulk NaCl/SDS mixtures and the corresponding nanoparticles are in disagreement with each other at high SDS volume fractions (Table 4). SDS/NaCl nanoparticles that are at $\chi_{NaCl} < 0.92$ (assuming ZSR-derived composition) display mutual deliques-

TABLE 4: SDS/NaCl Nanoparticle Composition Results from ZSR Modeling

expected composition from solutions						calcd composition from ZSR model						
wt/wt % SDS/NaCl	χ_{NaCl}	ε_{NaCl}[a]	d_{NaCl} (nm)[b]	Δ_{SDS}(nm)[c]	a_w[d]	wt/wt % SDS	χ_{NaCl}	ε_{NaCl}[a]	d_{NaCl} (nm)[b]	Δ_{SDS}(nm)[c]	a_w[d]	DRH (% RH)[e]
0	1.00	1.00	14.0	0.0	0.764	0	1.00	1.00	14.0	0.0	0.764	78.5
5.0	0.99	0.90	12.1	1.0	0.748	14	0.97	0.75	10.0	2.0	0.756	79.5
11	0.98	0.80	10.6	1.7	0.756	40	0.88	0.42	7.0	3.5	0.828	76.8
23	0.94	0.62	8.7	2.7	0.747	67	0.71	0.19	4.9	4.6	0.931	70.7
50	0.83	0.33	6.2	3.9	0.835	90	0.36	0.05	3.0	5.5	0.975	−

[a] NaCl volume fraction of a dry particle. [b] NaCl core diameter calculated from previous methods (eq 7).[5] [c] Deduced thickness of SDS film: $(14.0 - d_{NaCl})/2$. [d] Measured activity of a bulk solution corresponding to the listed composition. [e] Measured deliquescence point of nanoparticles (or the end point of the gradual deliquescence transition).

cence at lower values of activity in comparison to pure NaCl nanoparticles. On the contrary, NaCl/SDS bulk mixtures at $\chi_{NaCl} < 0.92$ result in greater water vapor activities relative to a pure saturated NaCl solution. Because activity is a colligative property,[26] this would imply SDS is more miscible with NaCl in the nanometer regime as opposed to the bulk regime. An alternative and more likely interpretation is that the presence of SDS greatly affects the values of surface tensions at the NaCl(solid)−H_2O(adsorbed) and H_2O(adsorbed)−H_2O(gas) interfaces, which are theoretically predicted to have a large effect on the deliquescence phase transition in NaCl nanoparticles.[12] Regardless of the explanation, this dramatic change in the deliquescence behavior from the bulk to the nanoparticles is a clear manifestation of the importance of interfacial molecules in thermodynamic phase transitions experienced by nanoparticles.

XPS Characterization of SDS/NaCl Nanoparticles. Our hypothesis that SDS/NaCl nanoparticles are enhanced in SDS prompted us to investigate their composition using XPS methods. Absolute determination of the SDS coverage is not experimentally attainable from the information presented in Figure 4. However, a qualitative assessment of the nanoparticle surface can be made as XPS is a surface sensitive technique. The entire depth of sample is irradiated by X-rays; however, photoelectrons are collected from a relatively small depth in the sample due to inelastic scattering of photoelectrons. The inelastic mean free path (IMFP) of an electron through NaCl with 1300 eV kinetic energy is roughly 3.5 nm.[66] The Al source produced 1456 eV photons and the binding energy of Cl(2p) is ∼200 eV, thus the majority of electrons collected for NaCl would originate roughly 3.5 nm deep into the sample if no SDS existed on the surface. IMFP through aliphatic chains of the sort found in SDS is roughly 4.0 nm for an electron which has 1300 eV kinetic energy.[67] The binding energy of S(2p) is ∼170 eV; therefore photoelectrons could be collected through an SDS film thickness of ∼4.0 nm.

A simplistic core−shell model, in which a NaCl core floats in the middle of an SDS shell, predicts that the ratio S(2p)/Cl(2p) should increase more rapidly than linear (almost exponentially) with the SDS weight fraction. Above the SDS film thickness of 4 nm, nearly all Cl(2p) photoelectrons from the NaCl core should be inelastically scattered and thus not detectible. Table 4 shows that the particles examined by XPS have an SDS thickness ranging from 0 to 3.9 nm or 0 to 5.5 nm depending on whether one assumes the solution composition or ZSR composition for the nanoparticles. The S(2p)/Cl(2p) ratio should increase greatly over this range of SDS coat thicknesses. Figure 4 demonstrates that the measured S(2p)/Cl(2p) signal increases less than linearly with increasing SDS weight fraction. These observations suggest the core−shell morphology is not the best picture at high SDS weight fractions.

The XPS results are more consistent with a "zone-inclusion" model, whereby NaCl and SDS still segregate in separate phases but the NaCl zone is no longer in the very center of the nanoparticle as the core−shell model assumes. With the NaCl zone positioned near the edge of the particle, the Cl(2p) photoelectrons originating from NaCl could be fairly close to the surface and detectible by XPS. Note that the zone-inclusion model is just as consistent with the hygroscopic growth results as the core−shell model.

FTIR and AFM Characterization of SDS/NaCl Nanoparticles. The phase state of SDS in the nanoparticles dominated by SDS (23 and 50 wt/wt %) is uncertain. Some of the possibilities include (1) a glassy state with the alkyl chains being fairly disordered and (2) a crystalline state with a higher degree of order. All known crystalline forms of SDS pack head-to-head and tail-to-tail; however, because of chain tilting stronger bonding occurs between tails and hence the growth rate for the monohydrate and hemihydrate forms are much faster than the 1/8 hydrate and anhydrous forms.[68] If SDS is in a crystalline state, the 23 and 50 wt/wt % SDS/NaCl nanoparticles are likely to be of the monohydrate variety as the habit of this crystal domain is rectangular and ideally could pack well with the cubic NaCl crystal habit.

The 23 wt/wt % SDS/NaCl nanoparticles were examined by FTIR because this composition should have well in excess of one monolayer of SDS. FTIR spectra were difficult to obtain due the small amount of material impacted on the ZnSe window. However, the resulting spectra in the CH-stretching range (Figure 5) were quite informative. Most significantly, the symmetric and asymmetric $-CH_2-$ stretches, occurring at 2848 and 2918 cm^{-1}, respectively, are quite narrow, indicating minimal heterogeneous broadening of the peaks.

FTIR spectra of various SDS phases (crystalline and disordered) have been reported previously.[69] The position of the symmetric $-CH_2-$ stretch is consistently below 2852 cm^{-1} for crystalline phases of SDS, while that for micellar solutions of SDS and water is consistently above 2852 cm^{-1}.[69] The position of the asymmetric $-CH_2-$ stretch is just at or below 2920 cm^{-1} for crystalline phases of SDS, while for micellar solutions and liquid crystal phases of SDS is above 2920 cm^{-1}.[69] The position of the peak relative to 2920 cm^{-1} is not necessarily a function of order, but can also be related to packing density.[69] In disordered SDS phases, (i.e., micelles and liquid crystals) broadening of symmetric and asymmetric $-CH_2-$ peaks was observed relative to ordered, crystalline SDS phases (i.e., SDS anhydrous, $SDS\cdot{}^1/_8H_2O$, $SDS\cdot{}^1/_2H_2O$, and $SDS\cdot H_2O$) as well as a decreased molar absorptivity of the asymmetric $-CH_2-$ stretch relative to the symmetric $-CH_2-$ stretch.[69] The FTIR spectra presented in Figure 5 in this work appears to be more representative of an ordered, crystalline phase of SDS with high packing density.

AFM images of the sort shown in Figure 6 suggest that 23 wt/wt % SDS/NaCl nanoparticles are uniform and spherical. Higher resolution (0.5×0.5 μm) images were acquired (data

not shown) to confirm that. Those images revealed no irregular or peculiar features on the nanoparticles. Within the framework of the zone-inclusion model, these images suggest that (i) both NaCl and SDS inclusions pack with similar geometry and (ii) NaCl crystal is not expelled to the surface of SDS (or vice versa).

It is peculiar that AFM images suggest 23 wt/wt % SDS/NaCl nanoparticles are spherical yet the FTIR spectrum presented in Figure 5 suggests that SDS is in a crystalline state. These differences may reflect the large effect of the residual water on the morphology of SDS (see Zelenyuk et al.[21]). The conditions used to characterize the nanoparticles were quite different. For example, the AFM measurements were done under ambient RH, whereas FTIR and XPS spectra were taken under very dry conditions. In the hygroscopicity experiments, the SDS/NaCl nanoparticles were diffusion dried for a very short time (~1 s), whereas in the FTIR analysis nanoparticles were exposed to dry air for several days. The phase state of SDS in nanoparticles could potentially be different in all of our experiments. This should be kept in mind when interpreting data presented in this work.

Conclusions

A combination of experimental and theoretical techniques has been used to explore hygroscopic growth of 14.0(±0.2) nm NaCl and SDS/NaCl particles. Nanoparticles electrosprayed from a 5.0 wt/wt % SDS/NaCl solution deliquesce at the same RH where pure 14 nm NaCl nanoparticles deliquesce, at 79.1(±1.0)% RH. This composition also has the same water coverage level, 3.1(±0.5) ML, as pure NaCl nanoparticles do immediately prior to deliquescence. The estimated SDS surface coverage (Θ_{SDS}) for the 14 nm 5.0 wt/wt % SDS/NaCl particles is close to one monolayer, and this SDS monolayer does not appear to have a strong effect on the hygroscopic properties of the NaCl core. The molecular dynamics simulations of water uptake on the SDS-coated NaCl surface suggest that SDS kinetically hinders the initial adsorption of H_2O in the first few nanoseconds of the surface's exposure to water vapor. However, the experiment shows that H_2O penetrates through SDS film on the slow (seconds) time scale of the hygroscopic growth measurements. The presence of SDS on the surface in fact makes equilibrium adsorption of H_2O occur at lower RH than on bare NaCl because of the effect of SDS on the interfacial surface tension.

The situation changes considerably as the relative amount of SDS in the particle increases. XPS analysis suggests that nanoparticles with high SDS content deviate from the simple NaCl core−SDS shell morphology. *Ab initio* calculations reported in the work suggest that there is a strong energetic benefit for the SDS headgroups to interact with the NaCl surface, with the calculated binding energies on the order of 35 kcal/mol. However, above 1 ML coverage, there is simply not enough space to accommodate all of SDS on the surface and this leads to the growth of an SDS crystalline phase around the NaCl inclusion. The FTIR analysis reveals alkyl chains are fairly ordered in 23 wt/wt % SDS/NaCl, confirming that NaCl and SDS exist in segregated crystalline structures within the nanoparticle. As the relative amount of SDS in the nanoparticle grows, the deliquescence relative humidity decreases and the deliquescence transition becomes less well-defined. The effect of SDS on the deliquescence of NaCl appears to be much greater in nanoparticles than in the bulk NaCl/SDS mixtures of the same composition. This underscores the importance of interfacial properties in the phase transitions experienced by nanoparticles.

Acknowledgment. This study was supported by the National Science Foundation (grants CHE-0431312 and CHE-0909227). M.S.G. was supported by a grant from the Air Force Office of Scientific Research.

References and Notes

(1) Foster, M. C.; Ewing, G. E. *J. Chem. Phys.* **2000**, *112*, 6817.
(2) Finlayson-Pitts, B. J.; Pitts, J. N. *Chemistry of the upper and lower atmosphere: theory, experiments, and applications*; Academic Press: San Diego, CA, 2000.
(3) Hemminger, J. C. *Int. Rev. Phys. Chem.* **1999**, *18*, 387.
(4) Finlayson-Pitts, B. J.; Hemminger, J. C. *J. Phys. Chem. A* **2000**, *104*, 11463.
(5) Alshawa, A.; Dopfer, O.; Harmon, C. W.; Nizkorodov, S. A.; Underwood, J. S. *J. Phys. Chem. A* **2009**, *113*, 7678.
(6) Hameri, K.; Laaksonen, A.; Vakeva, M.; Suni, T. *J. Geophys. Res. D* **2001**, *106*, 20749.
(7) Hameri, K.; Vakeva, M.; Hansson, H.-C.; Laaksonen, A. *J. Geophys. Res. D* **2000**, *105*, 22231.
(8) Romakkaniemi, S.; Haemeri, K.; Vaekevae, M.; Laaksonen, A. *J. Phys. Chem. A* **2001**, *105*, 8183.
(9) Biskos, G.; Russell, L. M.; Buseck, P. R.; Martin, S. T. *Geophys. Res. Lett.* **2006**, *33*, L07801.
(10) Biskos, G.; Malinowski, A.; Russell, L.; Buseck, P.; Martin, S. *Aerosol Sci. Technol.* **2006**, *40*, 97.
(11) Biskos, G.; Paulsen, D.; Russell, L. M.; Buseck, P. R.; Martin, S. T. *Atm. Chem. Phys.* **2007**, *6*, 4633.
(12) Russell, L. M.; Ming, Y. *J. Chem. Phys.* **2002**, *116*, 311.
(13) Tang, I. N.; Munkelwitz, H. R. *Atmos. Environ. A* **1993**, *27A*, 467.
(14) Cruz, C. N.; Pandis, S. N. *Environ. Sci. Technol.* **2000**, *34*, 4313.
(15) Hansson, H. C.; Rood, M. J.; Koloutsou-Vakakis, S.; Hameri, K.; Orsini, D.; Wiedensohler, A. *J. Atmos. Chem.* **1998**, *31*, 321.
(16) Choi, M. Y.; Chan, C. K. *Environ. Sci. Technol.* **2002**, *36*, 2422.
(17) Svenningsson, B.; Rissler, J.; Swietlicki, E.; Mircea, M.; Bilde, M.; Facchini, M. C.; Decesari, S.; Fuzzi, S.; Zhou, J.; Moenster, J.; Rosenoern, T. *Atmos. Chem. Phys.* **2006**, *6*, 1937.
(18) Woods, E., III; Kim, H. S.; Wivagg, C. N.; Dotson, S. J.; Broekhuizen, K. E.; Frohardt, E. F. *J. Phys. Chem. A* **2007**, *111*, 11013.
(19) Chen, Y.-Y.; Lee, W.-M. G. *Chemosphere* **1999**, *38*, 2431.
(20) Chen, Y.-Y.; Lee, W.-M. G. *J. Environ. Sci. Health* **2001**, *A36*, 229.
(21) Zelenyuk, A.; Imre, D.; Cuadra-Rodriguez, L. A.; Ellison, B. *J. Aerosol Sci.* **2007**, *38*, 903.
(22) Petters, M. D.; Prenni, A. J.; Kreidenweis, S. M.; DeMott, P. J.; Matsunaga, A.; Lim, Y. B.; Ziemann, P. J. *Geophys. Res. Lett.* **2006**, *33*, L24806.
(23) Rinaldi, M; Facchini, M. C.; Decesari, S.; Carbone, C.; Finessi, E.; Mircea, M.; Fuzzi, S.; Ceburnis, D.; M., E.; Kulmala, M.; de Leeuw, G.; O'Dowd, C. D. *Atmos. Chem. Phys. Discuss.* **2008**, *8*, 19035.
(24) Rader, D. J.; McMurry, P. H. *J. Aerosol Sci.* **1986**, *17*, 771.
(25) McMurry, P. H. *Atmos. Environ.* **2000**, *34*, 1959.
(26) Raff, L. M. *Principles of Physical Chemistry*; Prentice Hall: Upper Saddle River, NJ, 2001.
(27) Tang, I. N.; Tridico, A. C.; Fung, K. H. *J. Geophys. Res.—Atmos.* **1997**, *102*, 23269.
(28) Pruppacher, H. R.; Klett, J. D. *Microphysics of Clouds and Precipitation*; Kluwer Academic: Boston, 1997.
(29) Bahadur, R.; Russell, L. M. *Aerosol Sci. Technol.* **2008**, *42*, 369.
(30) Bahadur, R.; Russell, L. M.; Alavi, S. *J. Phys. Chem. B* **2007**, *111*, 11989.
(31) Cinkotai, F. F. *Aerosol Sci.* **1971**, *2*, 325.
(32) Harmon, C. W. "Hygroscopicity of Amphiphilic Nanoparticles: The Role of Size and Composition". Ph.D. Thesis, University of California, Irvine, CA, 2009.
(33) De La Mora, J. F.; Hering, S. V.; Rao, N.; Mcmurry, P. H. *J. Aerosol Sci.* **1990**, *21*, 169.
(34) De La Mora, J. F.; Rao, N.; Mcmurry, P. H. *J. Aerosol Sci.* **1990**, *21*, 889.
(35) Phillips, J. C.; Braun, R.; Wang, W.; Gumbart, J.; Tajkhorshid, E.; Villa, E.; Chipot, C.; Skeel, R. D.; Kale, L.; Schulten, K. *J. Comput. Chem.* **2005**, *26*, 1781.
(36) Feller, S. E.; MacKerell, A. D. *J. Phys. Chem. B* **2000**, *104*, 7510.
(37) Ryckaert, J. P.; Ciccotti, G.; Berendsen, H. J. C. *J. Comput. Phys.* **1977**, *23*, 327.
(38) Essmann, U.; Perera, L.; Berkowitz, M. L.; Darden, T.; Lee, H.; Pedersen, L. G. *J. Chem. Phys.* **1995**, *103*, 8577.
(39) Morgenstern, M.; Michely, T.; Comsa, G. *Phys. Rev. Lett.* **1996**, *77*, 703.
(40) Morgenstern, M.; Michely, T.; Comsa, G. *Phys. Rev. Lett.* **1997**, *79*, 1305.
(41) Jungwirth, P.; Tobias, D. J. *Chem. Rev.* **2006**, *106*, 1259.

(42) D'auria, R.; Tobias, D. J. *J. Phys. Chem. A* **2009**, *113*, 7286.
(43) Mackerell, A. D. *J. Phys. Chem.* **1995**, *99*, 1846.
(44) Aikens, C. M.; Webb, S. P.; Bell, R. L.; Fletcher, G. D.; Schmidt, M. W.; Gordon, M. S. *Theor. Chem. Acc.* **2003**, *110*, 233.
(45) Frisch, M. J.; Head-Gordon, M.; Pople, J. A. *Chem. Phys. Lett.* **1990**, *166*, 275.
(46) Pople, J. A.; Binkley, J. S.; Seeger, R. *Int. J. Quantum Chem.* **1976**, 1.
(47) Dunning, T. H. *J. Chem. Phys.* **1989**, *90*, 1007.
(48) Woon, D. E.; Dunning, T. H. *J. Chem. Phys.* **1993**, *98*, 1358.
(49) Baker, J. *J. Comput. Chem.* **1986**, *7*, 385.
(50) Culot, P.; Dive, G.; Nguyen, V. H.; Ghuysen, J. M. *Theor. Chim. Acta* **1992**, *82*, 189.
(51) Helgaker, T. *Chem. Phys. Lett.* **1991**, *182*, 503.
(52) Fletcher, G. D.; Schmidt, M. W.; Gordon, M. S. *Adv. Chem. Phys.* **1999**, *110*, 267.
(53) Gwinn, W. D. *J. Chem. Phys.* **1971**, *55*, 477.
(54) *NIST Computational Chemistry Comparison and Benchmark Database*; Johnson, R. D. I., Ed.; September 14, 2006.
(55) Djikaev, Y. S.; Ruckenstein, E. *J. Chem. Phys.* **2006**, 124.
(56) Tang, I. N. *J Geophys Res-Atmos* **1997**, *102*, 1883.
(57) Socrates, G. *Infrared and Raman Characteristic Group Frequencies*, 3rd ed.; John Wiley & Sons Ltd: West Sussex, England, 2001.
(58) Adamson, A. W.; Gast, A. P. *Physical Chemistry of Surfaces*, 6th ed.; Wiley-Interscience: New York, 1997.
(59) Gregg, S. J.; Sing, K. S. W. *Adsorption, Surface Area and Porosity*, 2nd ed.; Academic Press: London, 1997.
(60) *International Critical Tables of Numerical Data of Physics, Chemistry, and Technology*; Washburn, E. W., Ed.; McGraw-Hill Book Co.: New York, 1926.
(61) Verdaguer, A.; Segura, J. J.; Fraxedas, J.; Bluhm, H.; Salmeron, M. *J. Phys. Chem. C* **2008**, *112*, 16898.
(62) Peters, S. J.; Ewing, G. E. *Langmuir* **1997**, *13*, 6345.
(63) Tsai, D. H.; Zangmeister, R. A.; Pease, L. F., III; Tarlov, M. J.; Zachariah, M. R. *Langmuir* **2008**, *24*, 8483.
(64) Tang, K.; Smith, R. D. *J. Am. Soc. Mass Spectrom.* **2001**, *12*, 343.
(65) Cole, R. B. *Electrospray Ionization Mass Spectrometry*; John Wiley & Sons Inc: New York, 1997.
(66) Tanuma, S.; Powell, C. J.; Penn, D. R. *Surf. Interface Anal.* **1991**, *17*, 927.
(67) Cumpson, P. J. *Surf. Interface Anal.* **2001**, *31*, 23.
(68) Smith, L. A.; Duncan, A.; Thomson, G. B.; Roberts, K. J.; Machin, D.; McLeod, G. *J. Cryst. Growth* **2004**, *263*, 480.
(69) Sperline, R. P. *Langmuir* **1997**, *13*, 3715.

JP909661Q